MAE 263: Bionic Systems Engineering

Final Project

Aged Plantarflexor Bionic Assistance Device

Fall 2025

Group 7:

Alizee Wouters

Joseph Chavez

Stephen Hubbs

Hannah Yared

Kyra Sunil

Introduction and Background

For this project, a bionic assistance system was designed to address age-related weakening of the plantarflexor muscles, particularly the gastrocnemius and soleus. These muscles play a central role in walking by generating over half of forward propulsion during the push-off phase of the human walking gait cycle [1]. With aging, weakened plantarflexor muscles reduce the ability to produce ankle torque and power at the moment when the body relies on these muscles most [1]. This loss of function contributes to slower walking speeds, higher metabolic cost, increased reliance on compensatory muscles, and a greater risk of balance deficits and falls [1].

Age-related plantarflexor decline affects a large population. More than 61 million adults over sixty experience measurable reductions in push-off ability, especially those with early frailty or limited balance. As propulsion weakens, gait becomes less efficient and everyday mobility becomes more difficult, which can restrict independence and reduce overall quality of life.

Existing treatments such as strength training, orthoses, and electrical stimulation offer only partial improvement and do not fully restore late-stance push-off. This created motivation to design a bionic assistance system capable of supplementing plantarflexor torque during the critical portion of the gait cycle when propulsion is needed most. Providing well-timed assistance has the potential to increase ankle power, reduce metabolic cost, and support safer and more efficient walking in older adults.

In this work, the biomechanics of plantarflexor impairment were modeled in OpenSim, the resulting changes in gait mechanics were quantified, an optimized assistive torque trajectory was developed, and an actuator system was designed to deliver that assistance. The final design brought together biomechanical modeling, actuator performance analysis, control considerations, and system-level engineering decisions to create a complete and targeted bionic assistance solution.

Part 1: Biomechanical Modeling

1.1 Pathology Selection and Motivation

This project focuses on age-related weakening of the plantarflexor muscles in the lower limb. This condition is widespread among adults over sixty and contributes to reduced propulsion, slower walking speed, elevated metabolic cost, and increased fall risk [1]. The pathology is well documented, affects muscle tissue directly represented in OpenSim, and presents a clear opportunity for biomechanical improvement through assistive torque. Existing interventions such as strength training and orthotic support offer only partial restoration of push-off, highlighting the need for a targeted bionic solution.

1.2 Physiological Basis and Biomechanical Impact

Aging weakens the gastrocnemius and soleus muscles, which directly limits the ability of the plantarflexor complex to generate ankle torque during late stance. As these muscles weaken, they must activate more aggressively to achieve the same mechanical demands, and additional compensatory effort is recruited from dorsiflexors and proximal muscles. These internal compensations do not alter the externally imposed kinematics in a CMC-driven simulation, but they substantially increase the energetic cost of producing the same gait pattern.

The total metabolic cost plot below illustrates these effects clearly: the aged plantarflexor model shows consistently higher metabolic power across the gait cycle, with the largest increases occurring during early stance, mid-stance, and especially during push-off, when plantarflexors normally contribute the majority of forward propulsion. The sharper peaks and greater variability in the aged curve reflect inefficient force production, increased reliance on compensatory muscle groups, and reduced mechanical economy. These differences quantify the functional burden created by plantarflexor weakness and highlight the late stance phase of the gait cycle as a target for the greatest bionic assistance benefit.

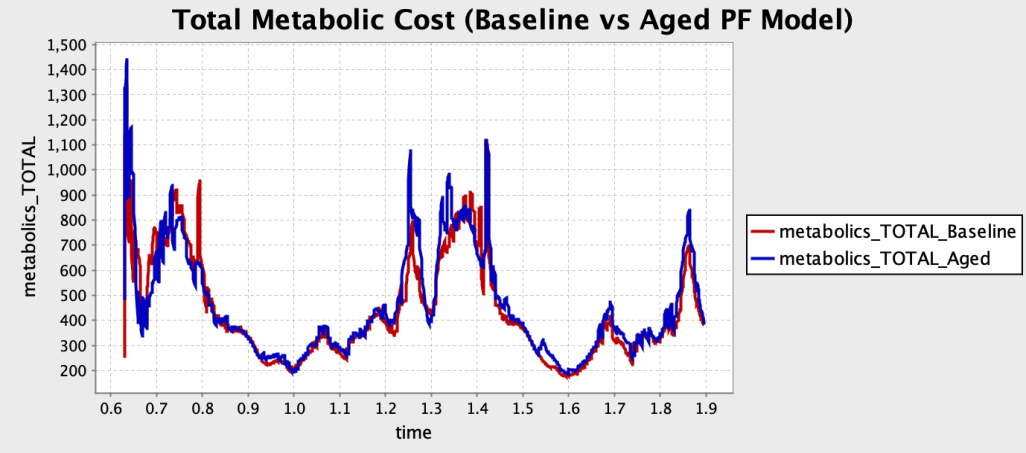

Figure 1. Total Metabolic Cost: Baseline vs Aged Plantarflexor Model

1.3 OpenSim Model Modification to Represent the Pathology

The aged plantarflexors pathology was modeled in OpenSim by modifying muscle properties in the gastrocnemius and soleus muscles of the Gait10dof18musc subject01_metabolics OpenSim model. The maximum shortening velocity (Vmax) of the gastrocnemius and soleus muscles was reduced from 10.0 to 6.0, representing a 40 percent decrease. This adjustment reproduces age-related declines in contractile speed [2] which contributes to reduced force-generation capacity in older adults, simulating the slower and weaker push-off observed in older adults.

The modeling workflow followed the standard sequence of Inverse Kinematics, Computed Muscle Control, and Inverse Dynamics so that comparisons between the baseline and aged models were controlled and consistent. Because both simulations tracked the identical joint kinematics, differences arose only from the altered plantarflexor properties. This ensured that changes in muscle activations, muscle forces, metabolic cost, joint moments, and joint power could be attributed specifically to reduced maximum shortening velocity (Vmax) rather than differences in movement. This approach isolates the mechanical effects of plantarflexor aging, producing realistic reductions in ankle torque and power that align with documented gait characteristics in older adults.

1.4 Outcome Measure Selection and Pathology Evaluation

Ankle push-off power and metabolic cost were chosen as the primary outcome measures because they directly capture the mechanical and energetic consequences of plantarflexor weakening. To evaluate the modeled pathology, CMC simulations were run for both baseline and aged plantarflexor models. Across all analyses, the aged model showed increased metabolic demand, elevated muscle activation and force requirements, reduced ankle moment generation, and more variable ankle power and work output, despite repeated joint kinematics enforced by the tracking controller. These results quantify the functional deficits introduced by plantarflexor weakness and identify where targeted assistance would be most beneficial.

The metabolic rate profiles for gastrocnemius, soleus, and tibialis anterior illustrate how aging alters energetic demand in individual muscles. The aged model exhibits higher metabolic power in all three muscles, with substantial increases in the soleus and gastrocnemius muscles during mid and late stance, and a marked rise in tibialis anterior immediately after heel strike likely due to reduced control of plantarflexion. These changes reflect compensatory recruitment needed to maintain gait mechanics.

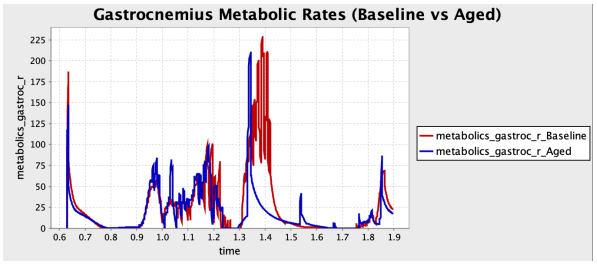

Figure 2a. Gastrocnemius Metabolic Rates: Baseline vs Aged

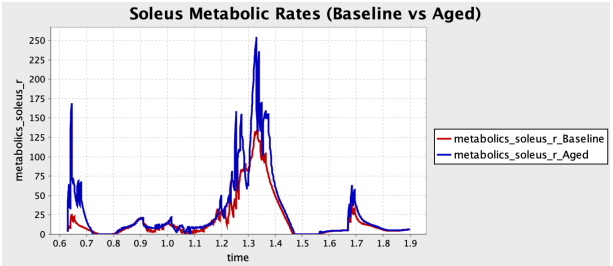

Figure 2b. Soleus Metabolic Rates: Baseline vs Aged

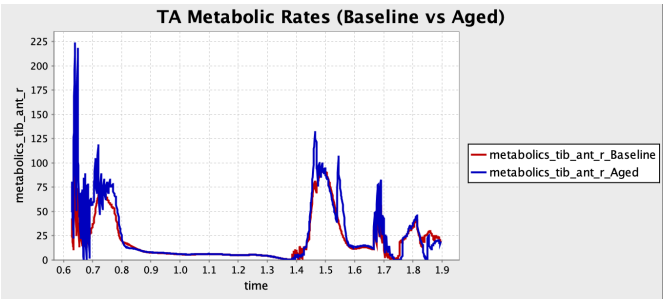

Figure 2c. Tibialis Anterior Metabolic Rates: Baseline vs Aged

The activation curves highlight neuromuscular compensation patterns. Both the gastrocnemius and soleus muscle require significantly higher activation during heel strike and stance, especially near push-off, to generate the required ankle moment with reduced contraction velocity. Tibialis anterior activation also rises sharply at heel strike as it works to prevent uncontrolled plantarflexion. These increases confirm that greater neural drive is required when plantarflexors weaken.

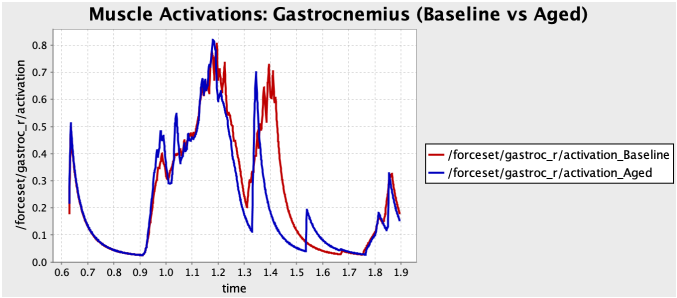

Figure 3a. Gastrocnemius Activation: Baseline vs Aged

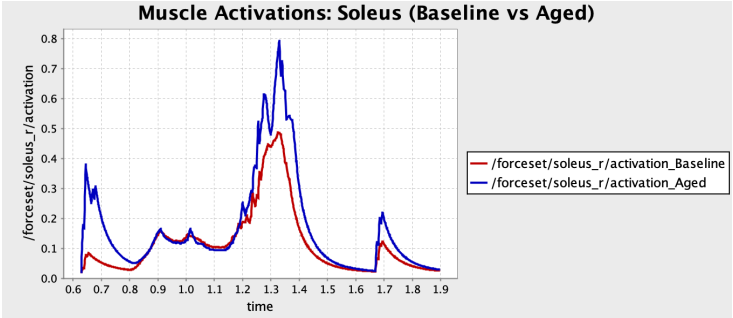

Figure 3b. Soleus Activation: Baseline vs Aged

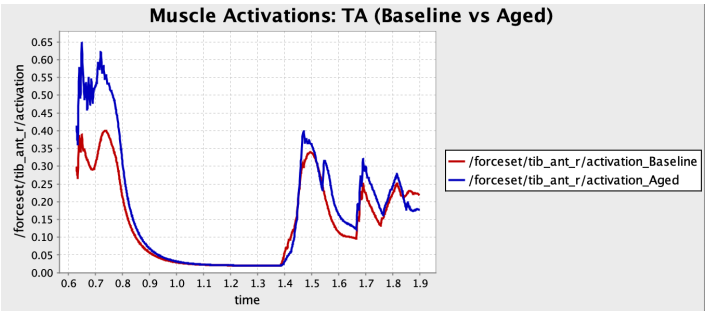

Figure 3c. Tibialis Anterior Activation: Baseline vs Aged

The muscle forces results show a similar pattern, with soleus muscle forces elevated throughout stance, with greatest increases near heel strike and terminal stance. The gastrocnemius muscle shows only small increases in muscle force during heel strike and after push off, indicating that most plantarflexor muscle force increase is in the soleus muscle. Tibialis anterior forces increase during early stance as the muscle compensates for insufficient eccentric control from weakened plantarflexors. These higher forces reflect both increased activation and reduced mechanical efficiency in the aged muscles.

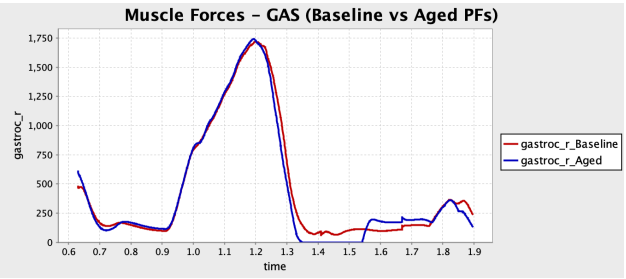

Figure 4a. Gastrocnemius Muscle Force: Baseline vs Aged

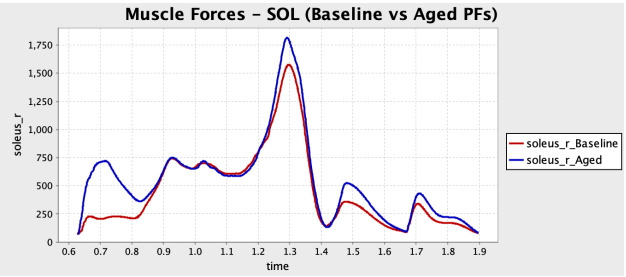

Figure 4b. Soleus Muscle Force: Baseline vs Aged

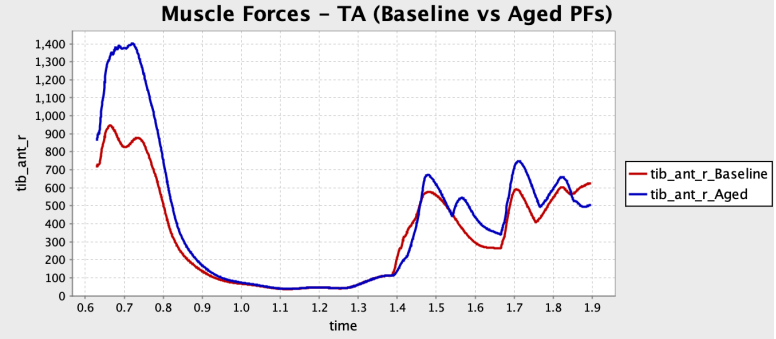

Figure 4c. Tibialis Anterior Muscle Force: Baseline vs Aged

Although internal muscle demands change substantially, the ankle angle trajectories match between the baseline and aged models. This results from the CMC enforcing the same experimental kinematics. The similarity in joint angle curves indicates that the effects of plantarflexor weakness arise from internal muscle effort changes rather than altered joint motion. Because both simulations follow identical kinematic targets, reduced plantarflexor capacity does not change the observed joint motion. Instead, the consequences of the pathology appear internally as increased muscle activation, higher metabolic cost, altered muscle forces, and reduced ankle moment and power.

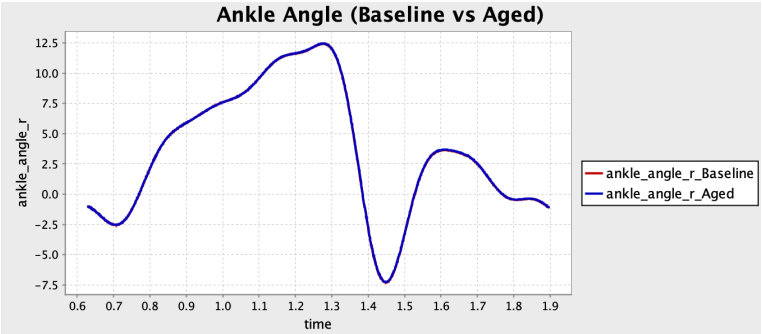

Figure 5. Ankle Joint Angle: Baseline vs Aged

The ankle angle trajectories for the baseline and aged models overlap almost perfectly across the entire gait cycle, reaching the same peak dorsiflexion during mid-stance and the same peak plantarflexion at push-off. This similarity is expected because both simulations were driven by identical experimental kinematics through inverse kinematics and CMC tracking. As a result,

joint motion is preserved even when plantarflexor strength is reduced. The effects of the pathology appear internally—as changes in muscle activation, force production, metabolic cost, joint moments, and joint power—rather than in the externally observed ankle angle trajectory.

The ankle moment curves clearly show the mechanical deficit introduced by plantarflexor weakening. The aged model produces a reduced peak plantarflexion moment during push-off and lower torque throughout mid-stance, reflecting diminished capacity to generate and control ankle propulsion. Early stance also shows a slight increase in dorsiflexor moment as the system compensates to stabilize the foot after heel strike when plantarflexor support is limited. These changes result in a less pronounced plantarflexor moment profile and altered early-stance mechanics consistent with compensatory patterns seen in age-related plantarflexor weakness.

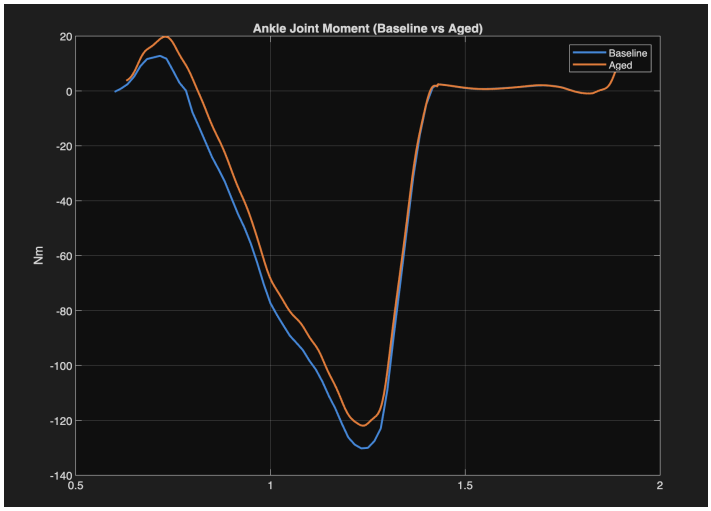

Figure 6. Ankle Joint Moment: Baseline vs Aged

The ankle power curves reveal a less efficient and more variable pattern in the aged model. Early in stance, positive power increases as compensatory muscles work harder to control tibial progression. Mid-stance shows spiked increases in negative power, indicating increased eccentric energy absorption when plantarflexor control is reduced. The most prominent change occurs during push-off, where the aged model exhibits a sharper and larger burst of positive power, reflecting the need to recruit the remaining plantarflexor capacity more abruptly to generate forward propulsion. Overall, the aged power profile is noticeably noisier and less smooth, demonstrating compensatory behavior characteristic of plantarflexor impairment.

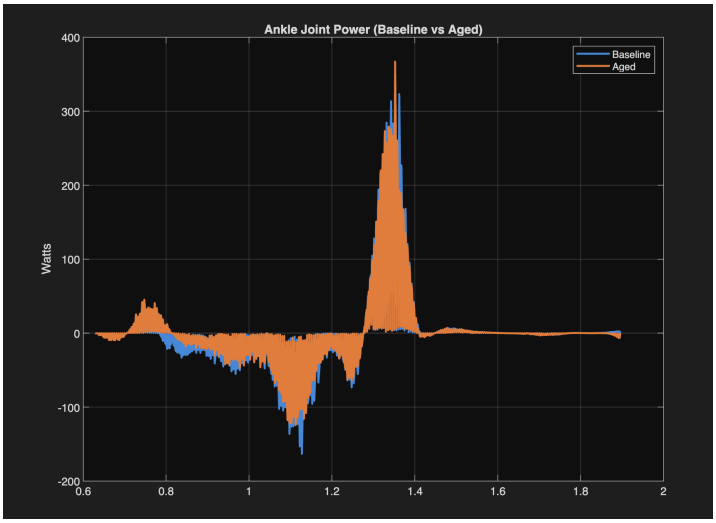

Figure 7. Ankle Joint Power: Baseline vs Aged Plantarflexor Model

Integrating ankle power over time shows that the aged model performs slightly more total positive mechanical work. The aged power curve is noticeably larger and much more spiky, with sharp bursts in both early stance and push-off instead of the smoother, broader peak seen in the baseline model. These abrupt power releases reflect compensatory effort when weakened plantarflexors cannot generate force efficiently. The increased variability and larger peaks indicate that the aged system must work harder and in a less efficient manner to maintain the same forward kinematics.

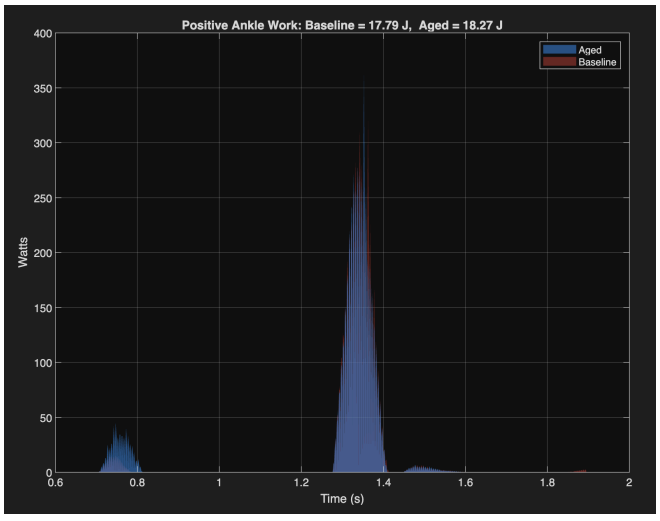

Figure 8. Positive Ankle Work: Baseline vs Aged Plantarflexor Model

Across all outcome measures, the aged plantarflexor model demonstrated a consistent pattern of reduced mechanical capacity and increased internal effort. Total metabolic cost rose due to higher reliance on compensatory muscles, and both gastrocnemius and soleus showed elevated activation and metabolic rates as they attempted to compensate for diminished force-generating ability. Muscle forces, particularly in soleus and tibialis anterior, increased to stabilize the ankle during early stance, even though the joint angle trajectory remained unchanged because the CMC enforced the same kinematics. Despite matching the same ankle motion, the aged model produced a smaller plantarflexor moment at push-off and a more variable, spiky power profile, including sharper bursts during both heel strike and propulsion. Positive ankle work was slightly higher as compensatory strategies added mechanical effort to maintain forward progression.

Collectively, these changes highlight the core deficits created by plantarflexor aging: reduced push-off torque, elevated metabolic demand, greater muscular effort, and inefficient power generation. These deficits directly inform the requirements for the bionic system. Assistance must target late stance where propulsion normally peaks, and supply enough torque to restore the reduced plantarflexor moment. By providing external push-off work, the device can offload the gastrocnemius and soleus muscles, reducing and smoothing metabolic cost and the ankle power profile, and replacing some of the compensatory mechanical work performed in the aged condition.

1.5 Conceptual Bionic System Design

The bionic system can be simply modeled as a pure torque source applied to the ankle. Although aging affects individuals bilaterally, only one side was modeled for simplicity. The system should be constrained to only apply force with plantarflexion, focusing on toe-off.

1.6 Implementation of the Bionic System in OpenSim

This system was modeled using the *CoordinateActuator* class within opensim. Using the scripting window, the actuator was created, the position was set at coordinate “ankle_angle_r”, and its torque was added to the joint. The torque was limited to negative values (plantarflexion) either by constraining the excitations through the control file or through the actuator settings.

Two different control mechanisms were used: utilizing the CMC tool to solve for the optimal actuator torque or the *controls_43p_r.xml* control file which is designed for plantarflexion assistance. While using the CMC tool, the actuator was limited to negative control values, whereas, the xml controls file was multiplied by a negative value which resulted in purely negative torque.

1.7 Optimization of Assistance Behavior

The two methods were tested while varying the actuator "optimal_force"; the metabolic cost was used to evaluate the effectiveness of the solution. Values of 45 and 100 were used for the CMC optimized solution, and values of -1.0, -3.0, and -5.0 were used for the xml controlled solution. The baseline (non-pathalogic) metabolic cost per step was 551 J, while the metabolic cost of the aged model was 575 J. Therefore, the motor should reduce the cost in the aged model to be nearer to baseline. The CMC optimized solution reduced metabolic cost to 561 J and 553 J for the 45 and 100 optimal_force values respectively. The xml control file solution reduced the metabolic cost to 569 J, 560, and 561 for optimal_force values of -1.0, -3.0, and -5.0 respectively. Therefore, the CMC optimized solution with an optimal_force of 100 reduced the metabolic cost closest to baseline, without exceeding the limit.

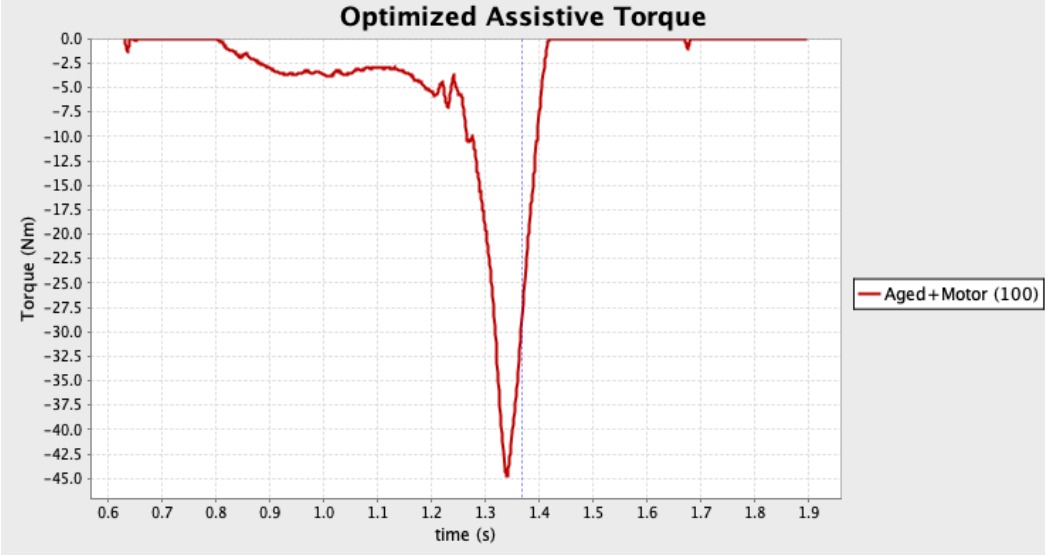

Figure 9. Optimized Assistive Torque Trajectory

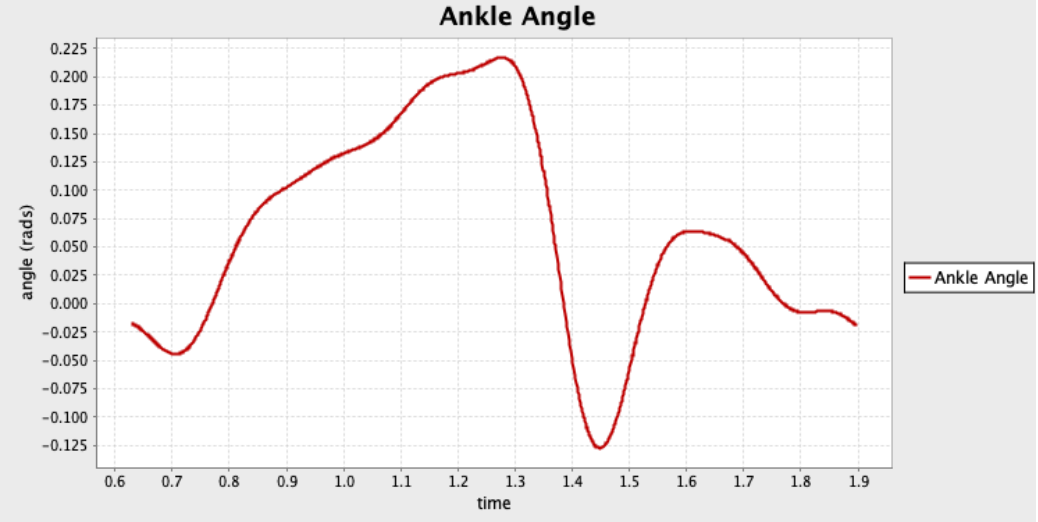

Figure 10. Optimized Assistive Angle Trajectory

These curves represent the selected assistance pattern applied during late stance. The torque rises sharply around 1.25 – 1.30 s, peaks in preparation of toe-off, and then rapidly declines, matching the timing of the plantarflexor deficit observed in the aged model. This profile provided the best balance between improving propulsion and maintaining stable gait mechanics, and it was used as the target trajectory for actuator design in Part 2.

1.8 Evaluation of the Optimized Bionic System

The optimized CMC simulations were evaluated to assess whether the actuator effectively compensated for plantarflexor weakness. The assisted model showed clear improvements in late-stance mechanics, with reductions in plantarflexor loading and metabolic effort during push-off. The residual forces and kinematics errors resulting from the RRA (reduce residuals algorithm) process show that the tracked motion fit the model well. The reserve actuator activation during CMC also remained low. These results indicate that the model is computationally stable and a good candidate for the types of simulations run.

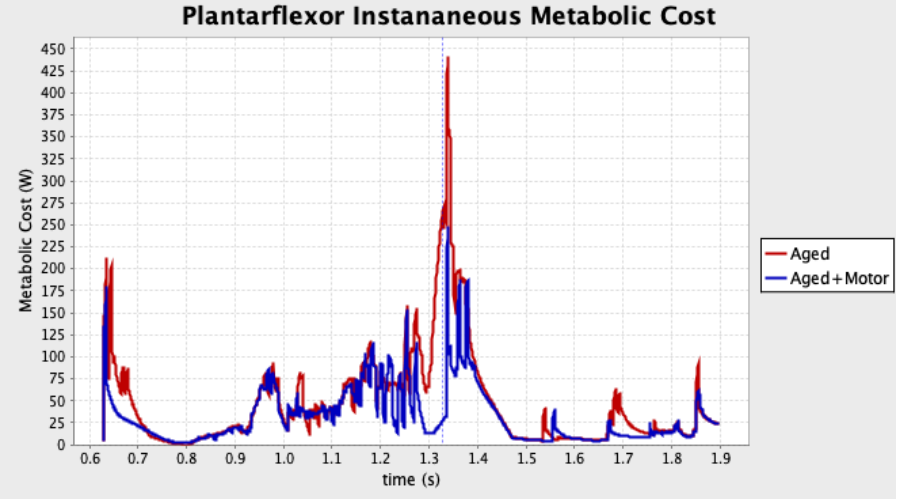

Figure 11. Instantaneous Metabolic Cost: Aged vs Aged+Motor

The modeled assistive device is shown above to drastically reduce instantaneous metabolic cost of the plantarflexor muscles during the gait cycle. Of note, the metabolic cost difference is highest during the pre-loading (~1.3-1.4 s) in preparation of toe-off. Since previous simulations proved the assistive device reduced total metabolic cost, these results prove that the device reduced the metabolic cost of the plantarflexor muscles specifically. Since, metabolic cost is the primary outcome measure of the model, the results demonstrate this has been achieved.

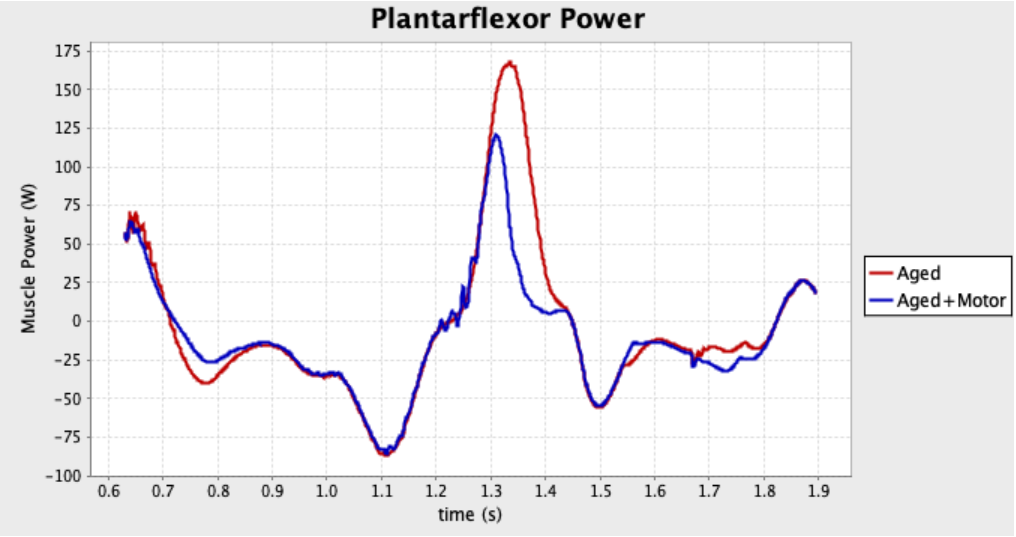

Figure 12. Plantarflexor Muscle Power: Aged vs Aged+Motor

In addition, the difference in power generated by the plantarflexor muscles was investigated for the aged/unassisted and aged/assisted models. Although this metric was not utilized in designing the device, the figure is still useful to demonstrate the reduction in power requirements from the plantarflexors. The metabolic cost metric shows the power consumed by the muscles when generating forces, whereas the power metric measures the power transferred to the joint. Since the motor is assisting by supplying power to the joint, this metric shows the most direct relationship between the motor and the muscles. The figure shows that the device targets assistance during toe-off, with little assistance during other phases, which should reduce the power requirements and price of the device.

Together, these results show that the optimized bionic system successfully lowered metabolic cost which was increased by muscle aging. Therefore, the model demonstrates that an assistive device for aged plantarflexor may be useful.

Since the model was built using a validate model, it was not necessary to re-evaluate the model's stability with regard to residual forces and kinematic errors. The results from the RRA are shown below which demonstrate that the model is stable. Only the errors relating to the right ankle are shown since that is the location of interest in the simulation. The kinematic errors remained below 1% of the range of motion of the angle (~20°), the average residual forces were all zero, and the average residual torques were all low. Therefore, the model motion is stable.

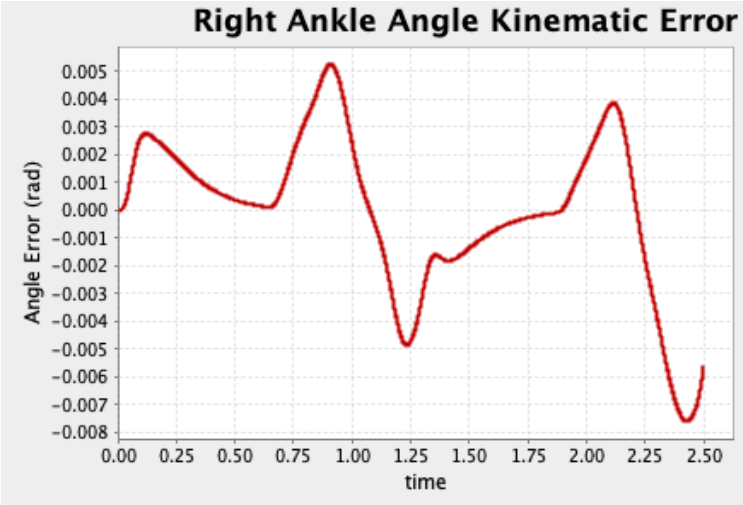

Figure 13a. Right Ankle Angle Kinematic Error

Average residuals:

• FX ≈ –3.78 N

• FY ≈ –2.78 N

• FZ = 0

• MX = 0

• MY = 0

• MZ ≈ –3.36 N·m

Next, the CMC results were evaluated for kinematic errors and reserve actuator activation. Again, the error was only evaluated for the right ankle. Kinematic error remained below 1% of the range of motion (20°) of the ankle during the simulations. Therefore, the ankle angle remained consistent and stable during the model simulations. Reserve actuation on the joint remained below 0.8% of the average torque on the joint for all simulations. This also demonstrates that the CMC simulations are stable for the model.

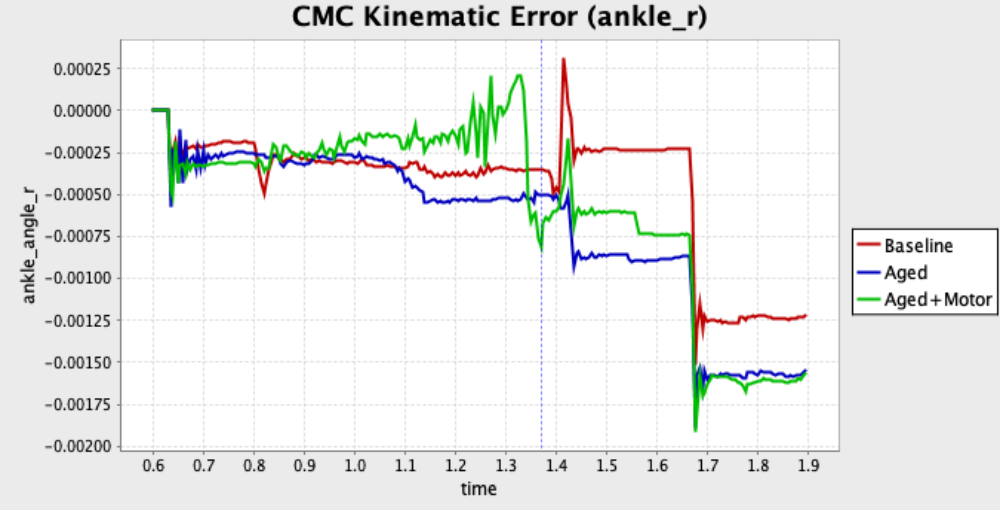

Figure 13b. CMC Kinematic Error: Baseline vs Aged vs Aged+Motor

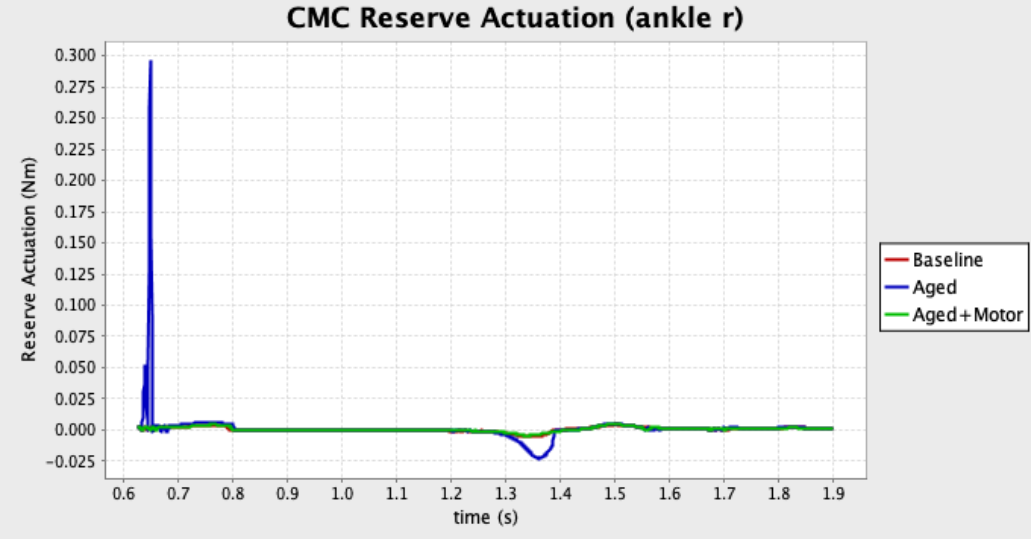

Figure 13c. CMC Reserve Actuation: Baseline vs Aged vs Aged+Motor

Collectively, the results of the error analysis and power analysis show that the model simulation is stable and the assistive device design is effective in achieving the goal of eliminating the increase in metabolic cost caused by aging of the plantarflexors. These findings confirm that the optimized bionic system provides meaningful biomechanical benefit and establishes a reliable foundation for the actuator and hardware design developed in the next phase of the project.

Part 2: Bionic System Design

2.1 Bionic System Design:

The proposed device is a plantarflexor bionic assistance system designed to restore push-off function and reduce metabolic cost by providing supplemental torque during late stance. It attaches to the user's leg through a two-part structure: a thin carbon-fiber footplate inside the shoe, anchored with straps over the dorsum of the foot (acting as a base for the ankle pulley), while a padded carbon-fiber shank shell wraps around the upper calf and houses the motor, gearbox, and electronics. These components are connected by an aluminum ankle hinge that integrates both the pulley and the series elastic element, as well as connects the shank piece to the footplate. When combined with a brushless DC motor and a cable-driven transmission

optimized to a gear ratio of approximately 250, the device can deliver the required 0-50 Nm of assistive torque while keeping distal mass low.

2.2 System Control:

At the high level, the controller specifies what category of behavior we want to produce in the limb. The goal is to restore ankle push-off power and reduce metabolic cost in older adults with reduced plantarflexor Vmax. Sensor signals from the IMU (SBG Pulse-40), ankle joint encoder (Broadcom AEAT-6012), and micro load cell (CZL611CD) are used here to determine where the user is in the gait cycle so that assistance is only considered during stance and particularly during late stance. This level decides that the limb should receive added push-off torque, but only in a way that supports natural, efficient walking.

At the mid level, the controller defines what joint dynamics are associated with that behavior. This is executed on the Teensy 4.1 microcontroller, which performs fast IMU processing and generates high-speed PWM signals for the motor driver. These capabilities allow the Teensy to produce smooth, precisely timed torque pulses that match the ankle's natural dynamics. Using sensor inputs, the microcontroller implements gait-phase–based control: heel strike resets the controller; midstance (~30–40% of gait cycle) begins the torque ramp; late stance (~45–60%) is where the assistive torque peaks between 40–50 Nm; and assistance stops at toe-off. The mid-level controller ensures smooth torque application and mimics natural ankle kinematics by shaping the torque profile according to the optimized trajectory from OpenSim.

At the low level, the controller answers how to deliver the appropriate amount of current to the motor to produce those desired dynamics. This is handled by the brushless DC motor (Maxon EC 60 24 V) with a series elastic cable-driven transmission and its motor driver (VESC 6). The torque command from the mid-level controller is converted into motor current using field-oriented control, with feedback from the motor and joint encoders and the series elastic element. A brushless DC motor is chosen over a brushed motor because it provides higher torque density (helping keep distal mass low), less wear (important for older users), higher efficiency and better thermal control, and it naturally supports precise phase-based torque control. It can

achieve the required 4 rad/s speed, 0–50 Nm torque, and late-stance assistance required by the design.

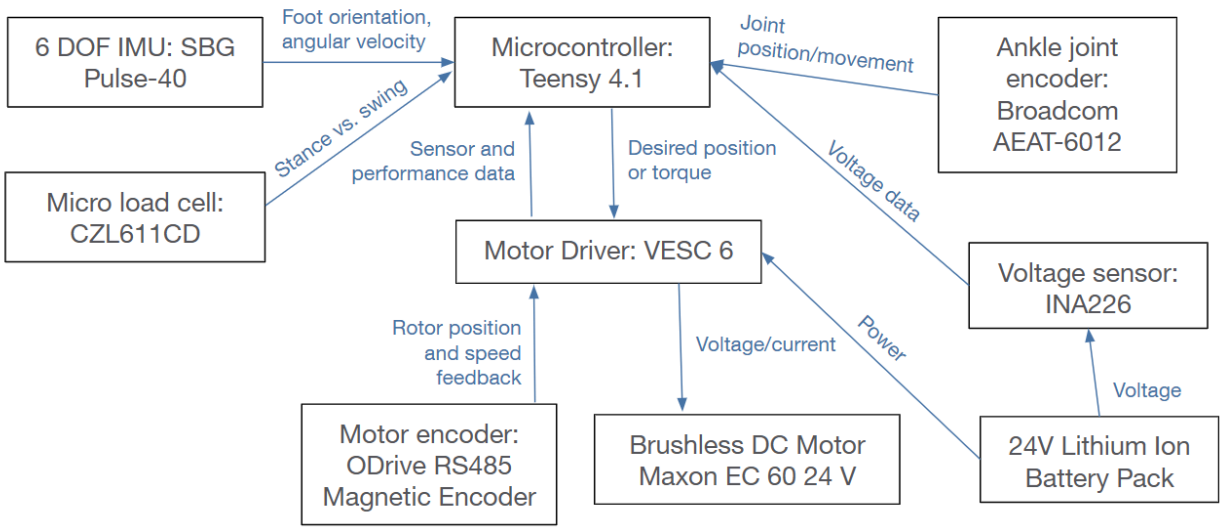

Figure 14: Communications Pipeline

2.3 Desired Torque and Angle Trajectory

The desired assistive trajectory for the bionic system was obtained directly from the optimized CoordinateActuator output generated in Part 1. This curve represents the actuator torque that most effectively restored plantarflexor function and reduced metabolic cost in the impaired model. Unlike the biological ankle moment, this trajectory reflects only the assistance supplied by the device, and therefore defines the exact torque–time profile the actuator must reproduce during walking.

The optimized assistance pattern consists of a smooth torque rise beginning in mid-stance, a peak of approximately 45 Nm during push-off, and a rapid decline at toe-off. This timing aligns with the period of greatest plantarflexor deficit in the aged model and captures the assistance window required to restore late-stance propulsion. Because this curve was generated through OpenSim's CMC optimization, it directly encodes both the magnitude and timing needed for effective bionic augmentation.

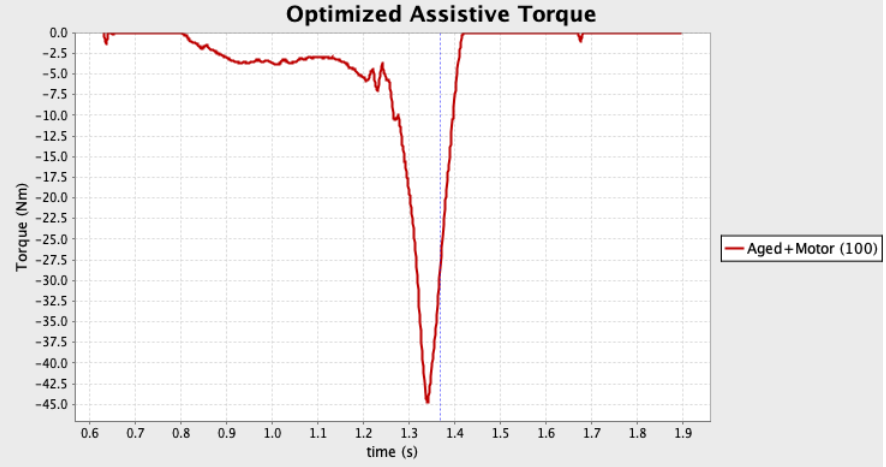

Figure 15. Desired Assistive Torque Trajectory

2.4 Motor Optimization and Transmission Ratio, Current Requirements and Heat Generated

After running an optimization between the motors (Table 1) in MATLAB, we learned that the best motor index was motor four, which corresponds to the Maxon EC 60 24V Brushless DC motor. Additionally, the simulation selected the optimal transmission ratio as 303:1, but only took into consideration the electrical requirements of the system. This would result in an extremely large gearbox and mechanical design. Therefore, we implemented mechanical constraints for the ratio and reran the simulation with values constrained between 100 and 250, in line with typical transmission ratios for ankle exoskeletons. This yielded an optimal ratio of 250:1, which is what we used going forward, as it provides the best compromise between electrical efficiency and mechanical constraints.

Motor	kT	Resistance	Induction	Inertia	Mass (g)	Voltage	Power (W)
1: RoboDrive ILM 50x08	0.058	0.54	4.90E-04	1.00E-05	87	48	209
2: RoboDrive ILM 50x08	0.062	0.604	4.90E-04	1.00E-05	76	48	215
3: Maxon EC 60	0.03	0.122	6.15E-05	1.25E-07	333	12	100
4: Maxon EC 60	0.114	1.09	8.64E-04	1.25E-07	333	24	100
5: Maxon EC 45	0.0451	1.25	6.91E-04	2.40E-05	143	30	70
6: Maxon EC 45	0.0533	1.83	9.66E-04	2.40E-05	143	36	70
7: Maxon ECX 22	0.0344	3.59	6.26E-04	7.63E-07	210	48	80

Table 1: Motor Optimization Table

To realize this ratio in hardware, we designed a cable-driven transmission in which the overall transmission ratio N is given by $N = G \cdot \frac{r_{ankle}}{r_{spool}}$, where G is the motor-side gearbox ratio, r_{ankle} is the ankle pulley radius, and r_{spool} is the motor spool radius. The calculation for the transmission ratio is displayed below. Because the maximum ankle rotation during assistance is only about 12 degrees of dorsiflexion, the change in moment arm is small, and the effective torque transfer remains approximately linear. At this angle, the delivered torque remains above 98% of its nominal value, so assuming a constant transmission ratio is appropriate for this design.

$$N = \frac{T_{ankle\ required}}{T_{motor}}$$

Defining N in this way accounts for both mechanical systems that make up our exoskeleton design. The following math aims to convert the required torques into measurable parameters.

$$T_{ankle\ required} = F_{cable}\, r_{ankle}$$

$$F_{cable} = \frac{T_{ankle\ required}}{r_{ankle}}$$

$$T_{spool} = F_{cable}\, r_{spool}$$

$$T_{spool} = \frac{T_{ankle\ required}}{r_{ankle}} * r_{spool}$$

$$G = gearbox\ ratio = \frac{T_{spool}}{T_{motor}}$$

$$T_{motor} = \frac{T_{spool}}{G}$$

$$T_{motor} = \frac{\frac{T_{ankle\ required}}{r_{ankle}} * r_{spool}}{G}$$

$$T_{motor} = \frac{T_{ankle\ required} * r_{spool}}{G * r_{ankle}}$$

$$N = \frac{T_{anke\ required}}{\frac{T_{ankle\ required} * r_{spool}}{G * r_{ankle}}}$$

$$N = G * \frac{r_{ankle}}{r_{spool}}$$

To identify a transmission ratio that balances efficiency and mechanical feasibility, electrical losses were computed for all candidate motors across a wide range of gear ratios. This analysis estimates how much electrical energy would be dissipated as heat while the actuator produces the required assistive torque trajectory. The results show that losses are high at both very low and very high gear ratios, but a clear minimum emerges in the mid-range. This optimum represents the most electrically efficient region where the motor operates with lower current demands and reduced resistive losses. The analysis supports selecting a gear ratio of

approximately 250:1, which falls near the efficient region while remaining mechanically practical for a cable-driven transmission.

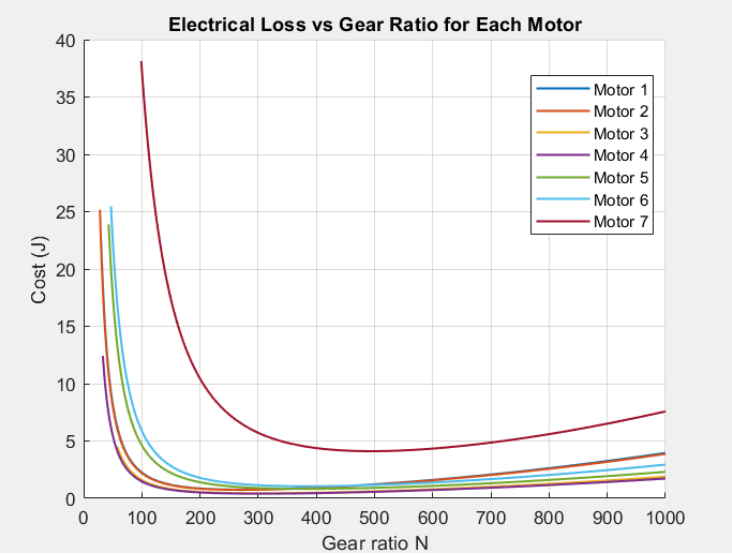

Figure 16: Electrical Loss vs. Gear Ratio for Each Motor

Once the optimal motor–gear ratio combination was selected, the current and voltage demands were evaluated to confirm that the actuator could feasibly reproduce the desired torque profile. The resulting current trace shows a brief peak during push-off, corresponding to the maximum torque demand, while remaining well below the continuous current rating of the motor. The voltage profile follows the same pattern and stays comfortably within safe operating limits. These results confirm that the selected motor can deliver the required torque and speed without electrical or thermal overload, supporting reliable long-duration operation during walking.

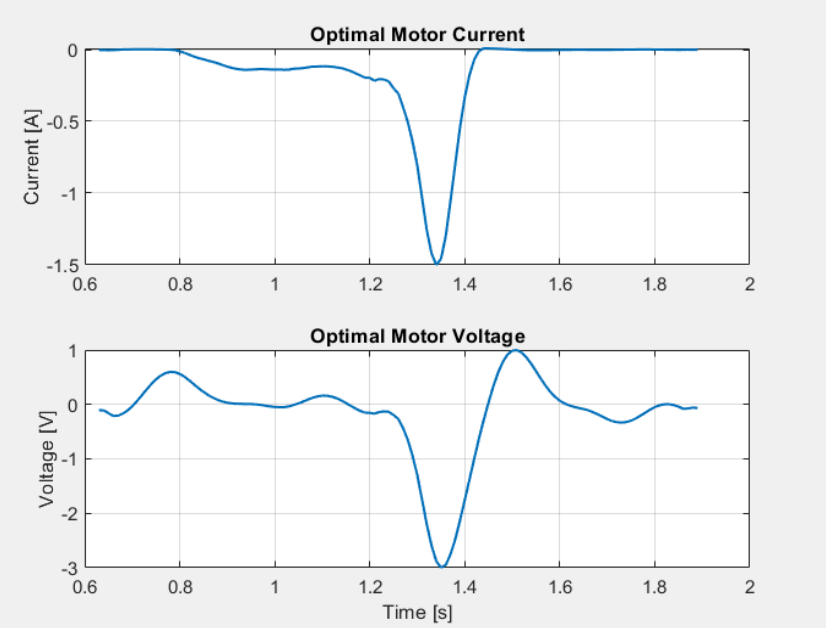

Figure 17. Motor Current and Voltage Requirements

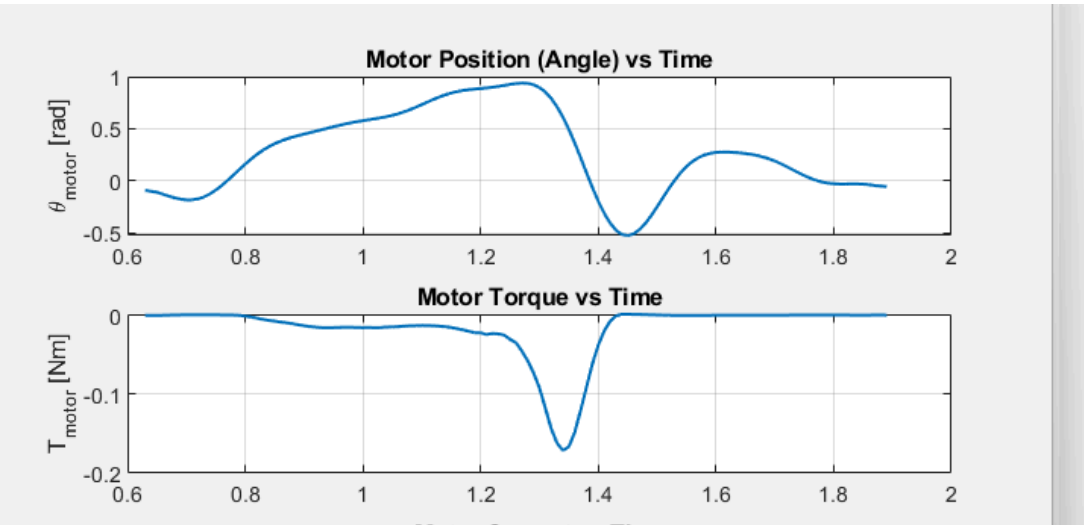

Figure 18. Motor Torque and Angle Trajectories

Looking at the root mean square current compared to the continuous current rating for the chosen motor, our system uses only around 7% of the current capability. This means the motor is understressed and can handle a long duration of use with minimal heating.

Similarly, the average copper loss is approximately 0.13 W for unilateral assistance, which is a very small heat load for a brushless DC motor of this size. This level of power dissipation can be managed entirely with passive cooling: the motor is mounted to an aluminum bracket that acts as a heat sink, and the actuator housing is vented to allow airflow. A thin padding layer between the actuator and the user's leg prevents any localized hot spots from being felt by the user. Overall, both the current levels and copper losses indicate that the motor will operate well within safe thermal limits during assisted walking.

2.5 Series Elastic Actuator:

A series elastic actuator (SEA) was added to the cable transmission because plantarflexor assistance must be delivered smoothly and in synchrony with the user's gait. The SEA provides compliance that helps store and return energy during push-off, filters rapid changes in torque, and reduces peak motor current by allowing small deflections under load.

To size the spring, the relationship $k=F_{max}/\delta_{max}$ was used, where F_{max} is the peak cable force corresponding to the maximum assistive torque and δ_{max} is an allowable deflection of ~3–5 mm. F_{max} was determined using $F_{max} = T_{max}/r_{spool}=3000$ N, where T_{max} was taken from Figure 10 to be 45 Nm and r_{spool} was 0.015 m. Allowing a small deflection of 3–5 mm yields a target stiffness range aligned with powered exoskeleton literature [3] of:

$k = 3000\ N/0.005\ m = 600{,}000\ N/m$

$k = 3000\ N/0.003\ m = 100{,}000\ N/m$

This stiffness balances torque transparency with beneficial compliance. Practically, the elastic element is placed inline with the transmission cable near the ankle pulley so that spring deflection can be inferred from the difference between motor and joint angles for torque control.

2.6 Battery:

$$E_{step} = \int_{t_0}^{t_1} P(t)dt = 0.488\,J$$

$$E_{daily} = 0.488\,J * 2500\ steps = 1220\,J$$

$$E_{daily,WH} = \frac{1220\,J}{3600} = 0.339\,Wh/day$$

$$E_{daily,WH,with\ 30\%\ efficiency} = \frac{0.339}{0.30} = 1.13\,Wh/day$$

$$Runtime, ideal = \frac{62.4}{1.13} = 55\ days$$

In line with the above calculations, we selected a 24 V, 2.6 Ah lithium-ion battery pack as the power source for the device. Although the battery is more than enough to satisfy the electrical requirements of the system, we went with a slightly larger and higher voltage system to power our motor selection. Based on the estimated energy consumption per day, this battery provides approximately fifty five days of intermittent walking assistance when assuming an overall system efficiency of 30 percent. This efficiency value is consistent with reported ankle exoskeleton performance, particularly those operating at high transmission ratios, and accounts for mechanical, electrical, and real-world losses.

2.7a Comms Hierarchy:

The communications pipeline for the bionic ankle system integrates the sensors, microcontroller, motor driver, and actuator into a unified control loop, as shown in Figure 18. Sensor data from the IMU, ankle joint encoder, and load cell are sent to the Teensy 4.1 microcontroller, which determines gait phase and computes the desired assistive torque. The Teensy communicates these torque commands to the VESC 6 motor driver, which regulates current to the brushless DC motor using encoder feedback to ensure accurate torque delivery. A

voltage sensor and battery module complete the system by providing power and monitoring electrical state. Together, these components establish a real-time, closed-loop control architecture that supports the high-, mid-, and low-level control structure described in Section 2.2.

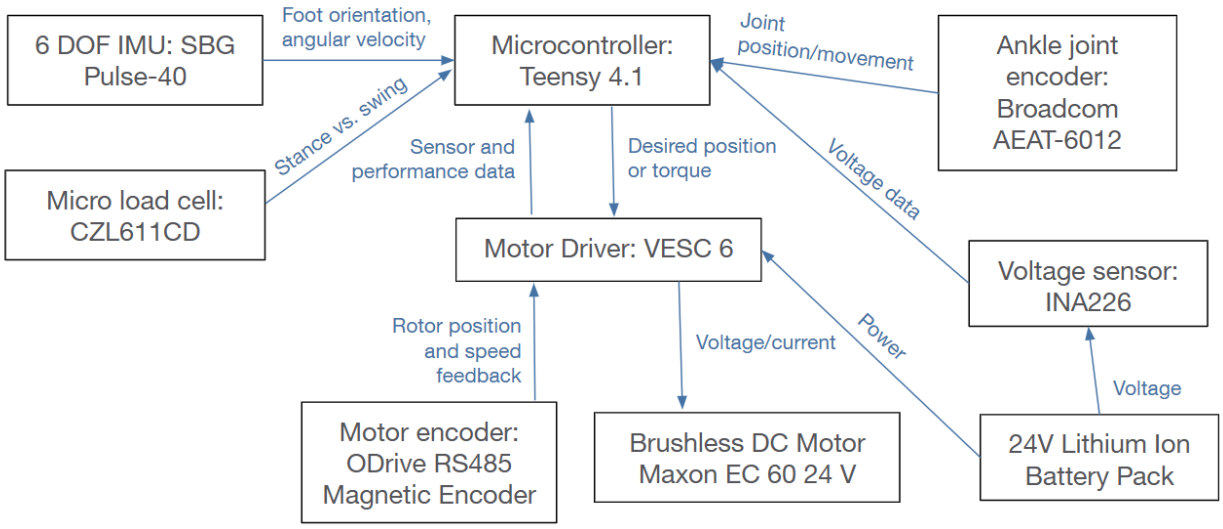

Figure 19: Communications Pipeline

2.7b Sensor and Electronics Selection:

The SBG Pulse-40 IMU was chosen over lower-grade MEMS units because it provides stable, high-quality measurements and is robust to vibration and motion, which is critical for foot-mounted sensing. The ODrive RS485 magnetic encoder was selected because it is highly resistant to vibration, dirt, and shock, making it more reliable than optical or less rugged magnetic encoders in wearable applications. A load cell was included because it provides clearer stance–swing detection than IMU-only methods, and a voltage sensor ensures safe battery monitoring.

The Teensy 4.1 microcontroller was chosen over alternatives for its fast IMU processing and high-speed PWM generation, enabling smooth, precisely timed torque commands while keeping mass low. Finally, the VESC 6 motor driver was selected for its built-in position, velocity, and torque control modes and reliable communication with the Teensy

(UART/CAN/PWM), offering smoother and more efficient torque control than simpler motor drivers.

2.8 Attachment System:

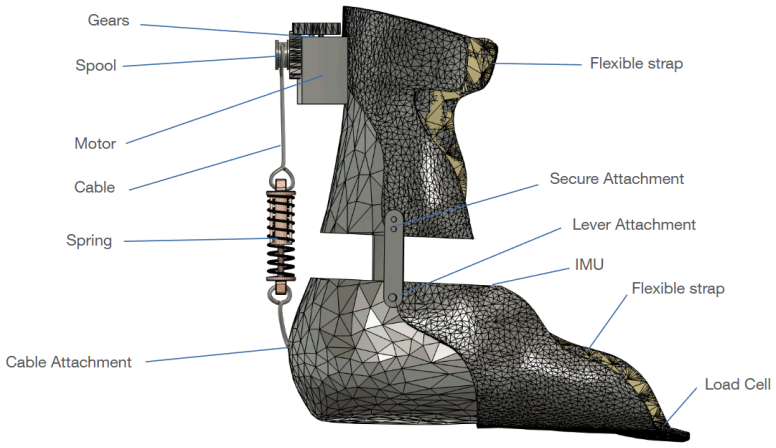

Figure 20: Bionic Assistance Device Design

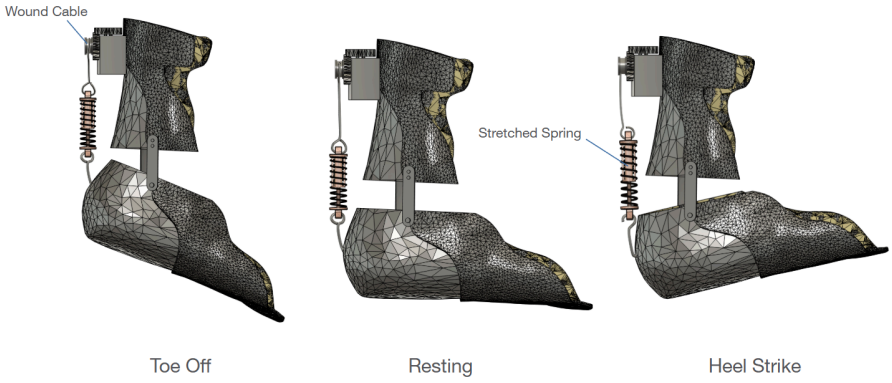

Figure 21: Bionic Assistance Device at Different Gait Phases

2.9 Mass Distribution and Integration Into OpenSim:

The device mass distribution is as follows:

- Total device mass: 1.185 kg (Battery 380g, MCU 10g, mass at the ankle)
- Device mass at the ankle: 0.795 kg (motor 333g, IMU 12g, Load cell 50g, motor encoder 6.3g, joint encoder 13.6g, motor driver 232g, device structure 125g, transmission 23.5g)

Calculating the device torque density:

- Torque density: Peak Torque / Device Mass = 45 N*m / 1.185 kg = 37.97 N*m/kg

The torque density was calculated to be 37.97 N*m/kg, indicating that the actuator delivers high assistive torque relative to its added mass.

To evaluate how the physical hardware affects gait mechanics, the mass of the bionic system was added to the OpenSim model and the simulation was rerun. The device mass at the ankle was added to the tibia and the remaining device mass was added to the pelvis. This was done to simulate the relative weights and their locations on the body.

After modifying these properties, CMC was rerun to check whether gait stability, tracking accuracy, or assistance effectiveness changed. The results showed that the leg continued to track joint kinematics accurately and that the optimized assistance profile still reduced plantarflexor loading during push off. Muscle coordination patterns remained similar to the previous simulation, indicating that the added hardware mass did not disrupt gait mechanics.

Kinematic errors and reserve actuator levels stayed within recommended OpenSim thresholds. This confirms that the model did not rely on artificial corrections and that the simulation remained physically consistent with the added mass.

However, since the model was strictly constrained by the motor activation, the CMC could no longer optimize the motor activation. This led to an increase in metabolic costs as the CMC increased activity of the nearby muscles to compensate for the constrained activation of the motor. Subtracting out the added metabolic cost from the constrained solution, the added mass of the device added ~7 J of energy expenditure per step. Overall, the re-run simulation demonstrated that the device mass is low enough to avoid degrading gait or negating the benefits of assistance. The bionic system remains feasible and effective when realistic hardware mass is included; however, the decrease in metabolic cost is likely insufficient to justify its use.

Part 3: Anatomical Engineering

3.1 Proposed Surgical Method

To enhance the effectiveness of the ankle exoskeleton, we propose surgically implanting an osseointegrated calcaneal anchor that would allow the exoskeleton to apply torque directly to the calcaneal. We would supplement the IMU and load cell with implanted intramuscular electrodes or tibial nerve cuffs that would provide higher fidelity motor intent signals.

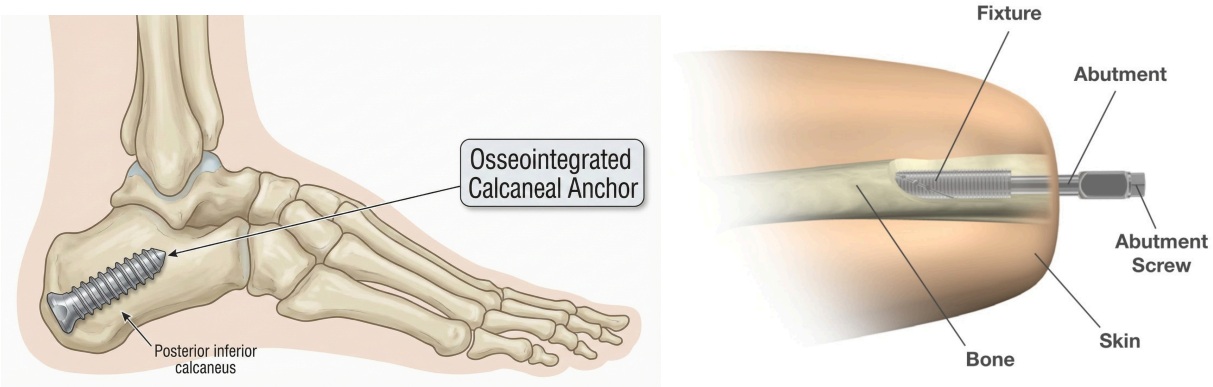

Figure 22: Osseointegrated Calcaneal Anchor

3.2 Cost–Benefit Analysis of the Invasive Method

Surgical Viability

The possibility of success for a surgically anchored exoskeleton system is supported by encouraging results from long term studies on osseointegrated prosthetic systems and implanted neural interfaces. Research has shown that patients with osseointegrated prosthetics can experience substantial improvements in prosthesis use, mobility, and overall quality of life. Hagberg et al. reported significant gains in self reported measures in both five year and ten year follow ups; “the prosthetic use score (+36), prosthetic mobility score (+18), problem score (−28) and global score (+38)” [4]. Brånemark et al. reported a five year cumulative osseointegrated fixture survival rate of 92% [5]. Neural cuff electrodes have also demonstrated safe and durable performance, with preserved nerve health and increased motor response. Freeberg et al. found

that “electrodiagnostics indicated preserved nerve health with strengthened responses following stimulated exercise,” [6] after nerve cuff integration. These findings indicate that the biological integration and neural interface components required for this system have already proven capable of supporting long lasting function and improving user experience.

3.3 Surgical Risks

Osseointegration research shows that infection at the skin interface is one of the most common complications, with skin infections ranging from 28% to 55% [7] and overall infection rates near 32% [8] across studies. Skin breakdown and ulceration also pose a moderate risk. Implant loosening or bone related stress injuries appear less frequently, but still meaningfully with rates of implant loosening at 2-6% and periprosthetic fractures at 0-9% [7]. The bone quality and load from the mechanical system significantly influence this risk. Although long term nerve health has generally remained preserved in nerve cuff studies, the neural implants introduce additional low to moderate risks, including minor perioperative nerve irritation and hardware malfunctions [6]. General surgical risks also apply, including anesthesia related reactions, bleeding, and wound complications. These events occur at relatively low rates in modern surgical practice, but should not be overlooked. Overall, soft tissue and infection related complications dominate the risk profile, while mechanical, neural, and surgical risks remain present, but less common.

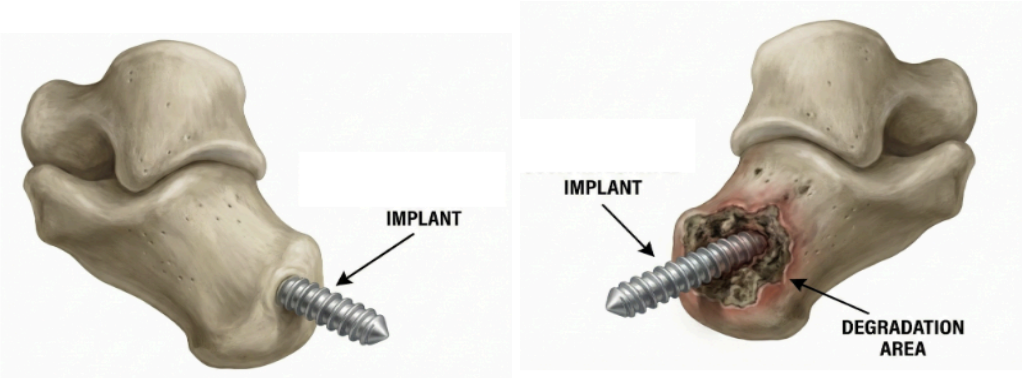

Figure 23: Osseointegrated Calcaneal Anchor Degradation

3.4 Qualitative Cost Benefit Analysis

Anchoring the device to bone may improve force transmission and direct torque application, while implanted nerve based sensing could reduce latency and enhance control. These electrodes can more accurately detect movement intent (e.g. gait changes, stairs, ramps) for more seamless transitions between environments. Users may also see improvements in comfort, such as reduced skin pressure, strap related irritation, slippage, and increased stability. These benefits stand against several significant drawbacks. The procedure requires surgery, recovery, and ongoing maintenance. There is a significant risk of health complications, especially of infection, associated with the procedure. Daily maintenance of the percutaneous site, activity limitations, and the presence of a visible implant also affect long term viability. Additionally, surgery, custom hardware, and implanted sensors carry significant financial burden. Overall, the limitations of this pathology and the benefits of the surgical integration do not outweigh the financial burden, health risks, and long term maintenance associated with surgical integration.

Conclusion

This project combined biomechanical modeling, actuator design, and control development to create a targeted bionic device for assisting age-related plantarflexor weakness. OpenSim simulations showed that reduced plantarflexor capacity increases metabolic cost and diminishes late-stance propulsion, guiding the development of an optimized assistive torque profile that restores ankle push-off without disrupting natural kinematics.

Using these insights, we designed a brushless DC motor system with a 250:1 cable-driven transmission and a series elastic element to deliver smooth, reliable 0–50 Nm torque assistance during late stance. A robust sensing and control architecture integrating an SBG Pulse-40 IMU, ankle encoder, ODrive magnetic encoder, Teensy 4.1, and VESC supports accurate gait-phase detection and precise motor actuation. Incorporating the actuator mass into the OpenSim model confirmed that the added hardware does not destabilize gait or diminish assistance effectiveness.

Overall, the system achieves the project's goal of creating a feasible bionic assistance device that can supplement plantarflexor function, reduce metabolic cost, and improve walking performance in older adults with weakened push-off.

References

[1] J. R. Franz, “The age-associated reduction in propulsive power generation in walking,” *Exerc. Sport Sci. Rev.*, vol. 44, no. 4, pp. 129–136, Oct. 2016, doi: 10.1249/JES.0000000000000086. Available: https://pubmed.ncbi.nlm.nih.gov/27433977/

[2] A. Kanayama, S. Yamamoto, R. Ueba, *et al*., “Age-related changes and sex differences in ankle plantarflexion velocity,” *Sci. Rep.*, vol. 13, 22943, 2023, doi: 10.1038/s41598-023-50275-1. https://www.nature.com/articles/s41598-023-50275-1

[3] J. Kim, S. Hwang, R. Sohn, Y. Lee, and J. Lee, “Development of an active ankle foot orthosis to prevent foot drop and toe drag in hemiplegic patients: A preliminary study,” *Appl. Bionics Biomech.*, vol. 8, no. 3–4, pp. 377–384, 2011, doi: 10.1155/2011/530375. Available: https://www.researchgate.net/publication/305509639_Development_of_an_Active_Ankle_Foot_Orthosis_to_Prevent_Foot_Drop_and_Toe_Drag_in_Hemiplegic_Patients_A_Preliminary_Study

[4] K. Hagberg, S. A. Ghasemi Jahani, O. Omar, and P. Thomsen, “Osseointegrated prostheses for the rehabilitation of patients with transfemoral amputations: A prospective ten-year cohort study of patient-reported outcomes and complications,” Journal of Orthopaedic Translation, vol. 38, pp. 56–64, Jan. 2023, doi: https://doi.org/10.1016/j.jot.2022.09.004.

[5] R. P. Brånemark, K. Hagberg, K. Kulbacka-Ortiz, Ö. Berlin, and B. Rydevik, “Osseointegrated Percutaneous Prosthetic System for the Treatment of Patients With Transfemoral Amputation: A Prospective Five-year Follow-up of Patient-reported Outcomes and Complications,” The Journal of the American Academy of Orthopaedic Surgeons, vol. 27, no. 16, pp. e743–e751, Aug. 2019, doi: https://doi.org/10.5435/JAAOS-D-17-00621.

[6] M. J. Freeberg, G. C. J. Pinault, D. J. Tyler, R. J. Triolo, and R. Ansari, “Chronic nerve health following implantation of femoral nerve cuff electrodes,” Journal of NeuroEngineering and Rehabilitation, vol. 17, no. 1, Jul. 2020, doi: https://doi.org/10.1186/s12984-020-00720-3.

[7] C. F. van Eck and R. L. McGough, “Clinical outcome of osseointegrated prostheses for lower extremity amputations,” Current Orthopaedic Practice, vol. 26, no. 4, pp. 349–357, 2015, doi: https://doi.org/10.1097/bco.0000000000000248.

[8] L. Diaz Balzani, M. Ciuffreda, G. Vadalà, G. Di Pino, R. Papalia, and V. Denaro, “Osseointegration for lower and upper-limb amputation a systematic review of clinical outcomes and complications,” Journal of Biological Regulators and Homeostatic Agents, vol. 34, no. 4 Suppl. 3, pp. 315–326. Congress of the Italian Orthopaedic Research Society, Jul. 2020, Available: https://pubmed.ncbi.nlm.nih.gov/33261296/.